Damage accumulation in braided textiles-reinforced composites under repeated impacts: Experimental and numerical studies

Chen Wang[a,b,c], Zhong Chen[b,*], Vadim V. Silberschmidt[c], Anish Roy[c]

[a] Joining Technology Group, Singapore Institute of Manufacturing Technology, 2 Fusionopolis Way, 138634, Singapore
[b] School of Materials Science and Engineering, Nanyang Technological University, 50 Nanyang Avenue, 639798, Singapore
[c] School of Mechanical, Electrical and Manufacturing Engineering, Loughborough University, Ashby Road, Loughborough LE113TU, United Kingdom

ABSTRACT

Composites reinforced with braided textiles exhibit high structural stability and excellent damage tolerance, making them very attractive for defence, aerospace, automotive and energy industries. Considering the real-life service environment, it is crucial to study a dynamic response of a composite structure and its energy-dissipation ability, especially under repeated low-velocity impacts. So, a series of drop-weight tests were carried out followed by X-ray computed micro-tomography to characterize damage morphology of braided composite specimens. Meanwhile, a multi-scale computational approach was explored and implemented as a user-defined-material subroutine (VUMAT) for ABAQUS/Explicit to capture main damage modes of a braided textile composite, while its delamination was modelled by employing cohesive-zone elements. Load- and energy-time curves were obtained both experimentally and numerically. The predicted levels of peak forces and absorbed energy were found to agree with the experimental data. An extent of delamination and damage accumulation in the braided composite was predicted numerically and analysed; it was found that material responses to repeated impacts had two types depending on the level of normalised impact energy. The presented modelling capability could contribute to design of braided composite structures for various applications.

Keywords:
Braided composite
Repeated low-velocity impacts
Damage accumulation
Energy absorption
Multi-scale modelling

1. Introduction

Composites reinforced with braided textiles are widely used in sports protective equipment, automotive components and aerospace structures thanks to their high structural stability and excellent damage tolerance [1]. For product design and optimisation purposes, dynamic behaviour of braided composite structures and their energy-dissipation ability should be well understood. As a consequence, studies of braided composites under low-velocity impact loads became important. In recent decades, numerous respective investigations have been carried out, remains the topic still challenging [1–4]. The main reason is the fact that failure associated with undulations and interlacing of the braided structure is difficult to deal with both in experimental measurements and finite-element modelling. Besides, typical damage modes caused by low-velocity impacts are barely visible in braided composites [4]. These features result in complex interactions between many stress and strain components.

In real life, structural materials are subjected to repeated impacts more often than single impact, during manufacturing, routine maintenance and daily service activities [5]. Although single impact generates only minor damage, these flaws can easily accumulate because of repeated impacts [6–8]. Thus, it is important to study such accumulating effects of repeated impacts on composite structures [9]. Comparing with many studies on the single-impact response, there are a few works concerning repeated impacts and damage accumulation [5,10,11]. Hosur et al. [5] studied the effect of stitching on a composite subjected to a certain number of repeated impacts with various impact energies. Belingardi et al. [12] developed an analytical model to describe a life time of composite materials subjected to repeated impact loadings. Atas et al. [9] presented an experimental investigation on a response to repeated impacts of woven E-glass/ epoxy composites with various thicknesses. Such studies about the behaviour of textile-reinforced composites after repeated impacts mainly focused on experiments. Additionally, there is a strong need to develop a FE approach capable of predicting dynamic behaviour of braided composites, considering different damage mechanisms, since experiments can be time-consuming and expensive. Although a few studies employed numerical simulations to establish the analytical model for glass/epoxy and fibre-metal laminates (FMLs), the shear-stress influence of the neighbouring layers on the interface delamination was not considered [2,3,10,13]. To

* Corresponding author.
E-mail address: ASZChen@ntu.edu.sg (Z. Chen).

the authors' knowledge, no FE model has been developed for braided composites to study their response to repeated impacts so far [14].

This work aims at investigating a response of a braided composite to multiple low-velocity impacts both experimentally and through FE simulations. A multi-scale computational approach was explored and implemented as a user-defined-material subroutine (VUMAT) for ABAQUS/Explicit to capture the main damage modes of braided textile composite. The results obtained with the developed computational model were compared to original experimental data for drop-weight tests. The resulting damage accumulation in braided composites is discussed. The presented modelling capability could contribute to design of braided composite structures for various applications.

2. Experimental procedure

A braided preform of the studied composite contained carbon-fibre tows (AKSAca A-42-12 k); a matrix material was Bakelite® EPR-L20 epoxy resin mixed with EPH-960 hardener at a weight ratio of 100:35, and the mixture was then degassed for approximately 30 min. The epoxy resin was injected into the preform employing a vacuum-assisted resin-infusion (VARI) method before curing for 24 h at room temperature followed by 15 h at 60 °C. The braiding angle in the laminates was 25° and a fibre volume fraction was about 55%. The plates were cut into pieces with dimensions of 55 mm × 55 mm × 1.6 mm; each plate consisted of two layers of the braided textile.

The drop-weight test programme was carried out with a 9250HV Instron Dynatup test system, as shown in Fig. 1. A spike-shape impactor was chosen considering real-life conditions of sports impact collisions between football shoes and shin-guards. The impactor had a flat bottom with a radius of approximately 5 mm (Fig. 1(b)) and a weight of 6.164 kg. The testing machine was equipped with an anti-rebound system to prevent multiple impacts on the tested specimen. The specimens were supported on a pair of pneumatically clamped rings with a 40 mm internal diameter. The low-velocity impact tests were carried out according to ASTM Standard D 7136. Before testing with repeated impacts, the perforation threshold of the braided composite plates (E_p) was evaluated, which was around 12 J in average. Then, repeated low-velocity impact tests were carried out with different impact energies

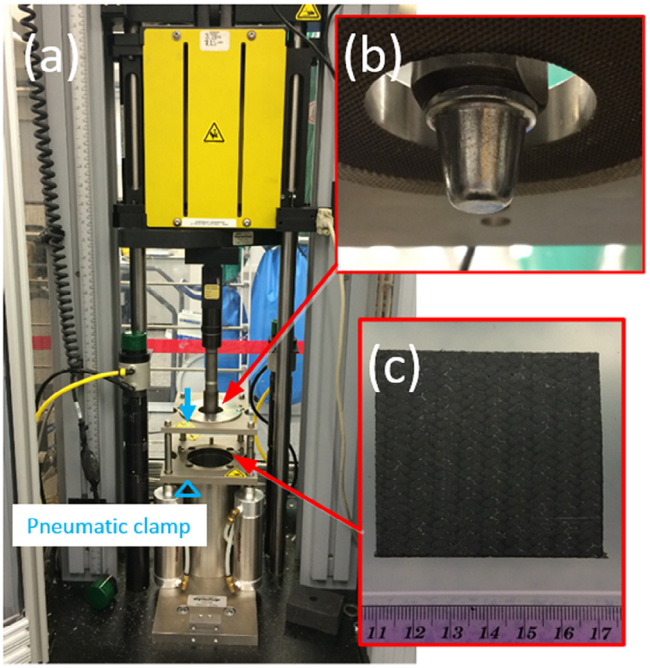

Fig. 1. (a) Drop-weight impact test setup with (b) spike-shape impactor and (c) plate braided composite specimen.

(2 J, 3 J, 4 J and 6 J); this was achieved by varying the initial height of the impactor with a constant mass. For each specimen, the impacts were repeated at least 20 times and stopped if perforation occurred. Five specimens were tested for accuracy at each impact energy level.

All the specimens were inspected post-test with X-ray micro-computed tomography (Micro-CT) measurements using a Metris 160H-XT XCT system to investigate the extent of the internal damage and delamination. Each scan was conducted at 60 kV and 150 μA using a tungsten target, with 2650 radiography projections taken over the 360° rotation for each specimen at an exposure of 500 ms.

3. Experimental results and discussion

3.1. Behaviour of braided composites under repeated impacts

The experimentally obtained load and internal energy responses of a braided specimen up to 20 repeated impacts with the impact energy of 2 J are shown in Fig. 2. For each impact, a roughly similar response was observed, and the impact duration time was identical. Under the first impact, oscillations of the load-time curve suggest the initiation of progressive failures in the material. After that, impact force has a relatively smooth curve with an increasing peak-load value. The energy-dissipation processes were also stable as shown in Fig. 2(b). The absorbed energies vary in a narrow range, indicating a slow damage-accumulation rate. Hence, braided composites performed robustly under repeated impacts with such a low impact-energy level.

In contrast, load- and energy-time curves of the braided composites under repeated 6 J impacts until final perforation exhibited another type of response: the peak load increased slightly after the first impact, then dropped down afterwards (Fig. 3). The sharp reduction of the impact force at the third strike is attributed to the occurrence of the fibre damage in yarns. The specimen dissipated more energy during successive impacts, leading to shrinkage of rebound energy. Once perforation occurs, there is no kinetic energy for rebound of the impactor. Hence, all of the impact energy is absorbed because of composite damage. It was also noticed that the engagement time between the composite and the impactor, governed by the friction forces and deflection, was longer with an increasing number of impacts.

In order to further investigate the effects of impact energy on braided composites under repeated impacts, the peak-force evolution was studied (Fig. 4). It can be observed that this peak increased during a few initial impacts as a result of a compaction process. The impactor contacted with a relatively softer matrix at the first few impacts and with the stiffer fibre-reinforced phase subsequently. The compaction process provides a stiffer surface with higher local fibre concentration for subsequent impacts, resulting in a higher peak load [15]. After the compaction, the peak force maintained a plateau for the impact energy of 2 and 3 J, indicating that at least 20 impacts were insufficient for fibre breakage and perforation. For impact energy higher than 3 J, a sharp reduction of peak force can be seen with an increasing number of impacts. Owing to propagation of damage and the stiffness loss, the maximum number of allowable impacts dropped down.

In addition, trends for impact-bending stiffness and maximum deflection during repeated impacts are presented in Fig. 5. The former was defined by the slope of the ascending section of the load-displacement curves; it represents the stiffness of composites under impact-induced bending in the beginning of the impact process. The maximum deflection means the maximum displacement of the impactor during each impact, reflecting the deformation of the composite specimen in the drop-weight test. For the impact energies of 2 and 3 J, it is obvious (Fig. 5) that the tested braided-composite plates have good impact resistances without a significant loss of bending stiffness. The maximum defection in these cases increased slightly with a similar rate. However, under impacts with energy larger than 3 J, the bending stiffness decreased dramatically, and the maximum deflection increased as a result of the bending-stiffness loss. The results also indicate that damage

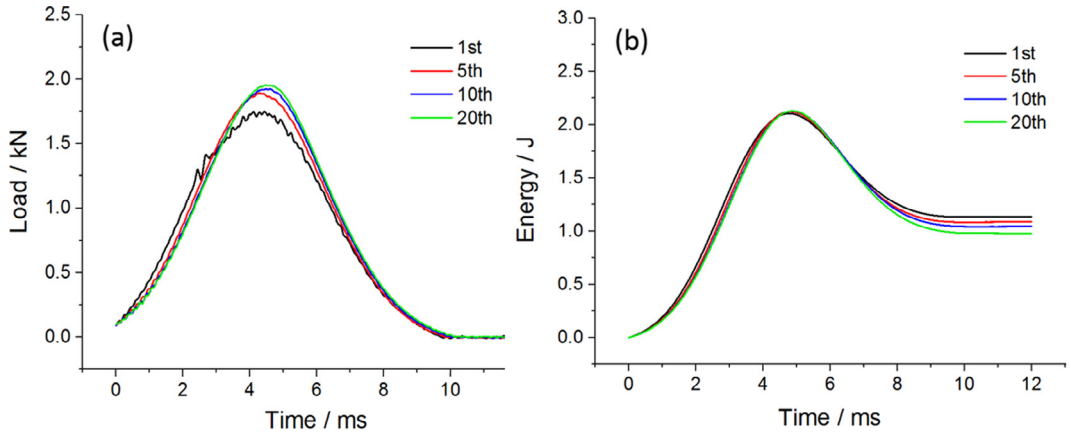

Fig. 2. (a) Load-time and (b) energy-time responses of braided composite plate under repeated 2 J impacts.

accumulation accelerated as the impact number increased.

According to Blingardli et al. [12], the normalised impact energy can be defined as the ratio of impact energy and perforation threshold (E_i/E_p) for a given material. Depending on the normalised impact energy, responses of the braided composite to repeated impacts can be classified into two groups based on the obtained results. In the first group, a low damage accumulation rate was observed when $E_i/E_p \leqslant 0.25$ (cases with impact energies of 2 J ($E_i/E_p = 0.17$) and 3 J ($E_i/E_p = 0.25$)). For another group, damage grew rapidly if $E_i/E_p > 0.3$ in this study (4 J ($E_i/E_p = 0.33$) and 6 J ($E_i/E_p = 0.5$)).

Differences of these two groups can also be reflected in terms of energy absorption. In a low-velocity impact, a part of the impact energy converts into the kinetic energy of the impactor's rebound, while another part is dissipated by a composite specimen. The fraction of absorbed energy is illustrated in Fig. 6. When $E_i/E_p < 0.25$, the absorbed energy decreased initially, then remaining nearly constant [15]. At the initial few impacts, the absorbed energy fraction decreased due to the compaction process with the specimen becoming tougher, less energy was able to dissipate at the ensuing impacts [16]. After the compaction process, the absorbed energy kept at a constant level, meaning that approximately the identical amount of energy was absorbed because of material damage for each impact. According to Fig. 6, more energy was absorbed after the second impact when $E_i/E_p > 0.3$. This was due to catastrophic damages taking place after a certain number of impacts. For instance, a quick damage accumulation might lead the fabric yarns on the back surface to fail in tension. A high damage-accumulation rate also corresponds to increased duration, lower peak load, and reduced stiffness. The perforation took place when the absorbed energy fraction was close to 1.

The term "damage accumulation" refers to evolution of damage in composites, specifically related to initiation, propagation or increase in density of cracks. It may also refer amount of energy that the system can dissipate. It is important to access the localization of impact-induced damage and design lay-ups and geometries of composites in order to optimise their structural behaviours. Two parameters were used to quantify damage accumulation by other authors. The one is the damage accumulation (DA) parameter introduced by Berlingardi [12,17], another is the damage index (DI) proposed by Amaro [18]. DA, monitoring a range of the penetration process in thick laminates, is also applied in case of repeated impact tests to get information on the rate of damage accumulation and on the onset of severe damage modes; It is defined as

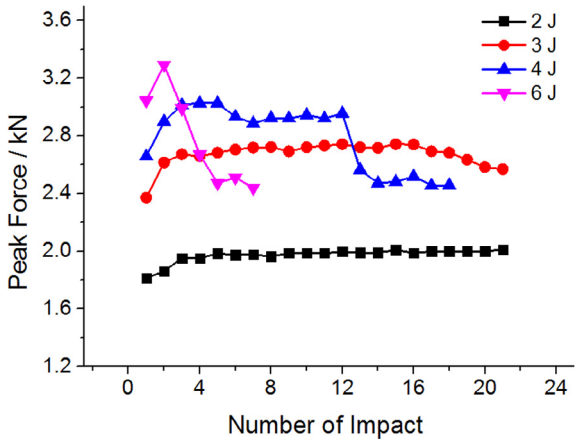

Fig. 4. Function of peak force with repeated impacts with different impact energies.

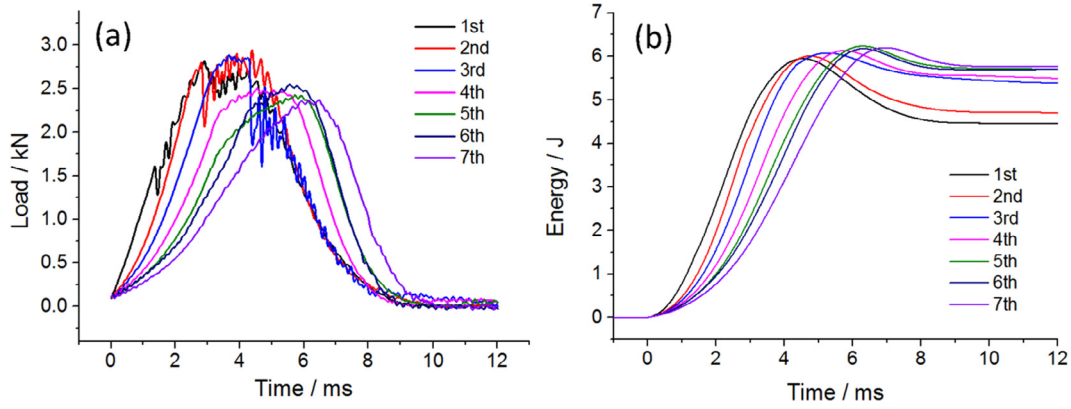

Fig. 3. (a) Load-time and (b) energy-time responses of braided composite plate under repeated 6 J impacts.

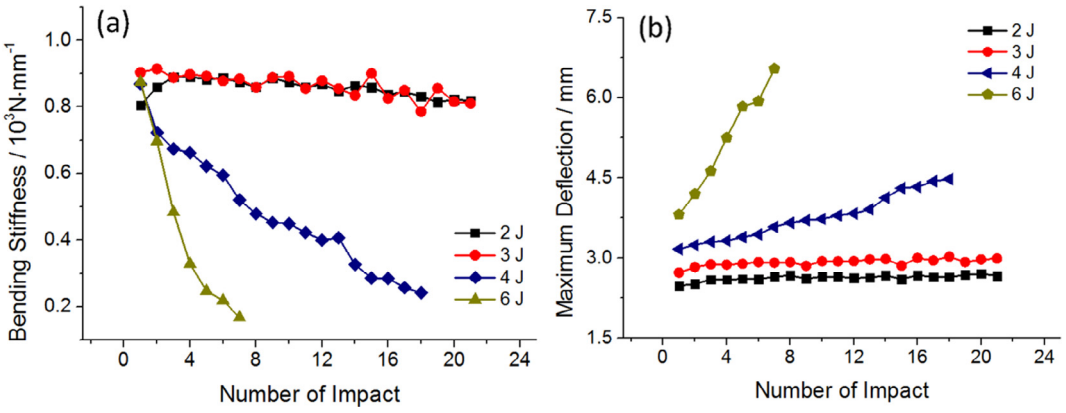

Fig. 5. (a) Bending stiffness and (b) maximum deflection of braided composites under repeated impacts with varying impact energies.

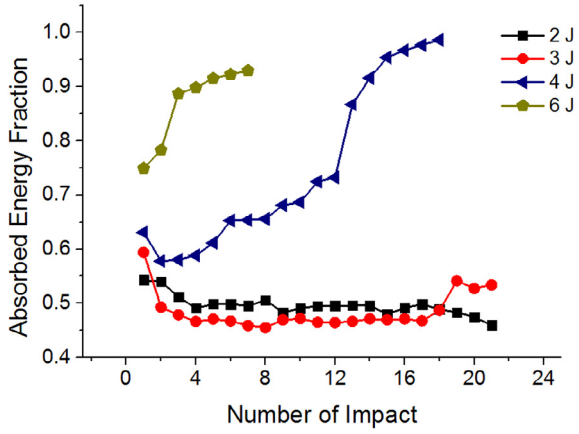

Fig. 6. Fraction of energy absorbed during repeated impacts with different impact energies.

$$DA = AEF\frac{\delta_{max}}{\delta_p}, \tag{1}$$

where δ_{max} is the maximum deflection for each impact (as shown in Fig. 5(b)) and δ_p is the critical deflection value at perforation (obtained from experiments) is the absorbed energy fraction (as presented in Fig. 6). *DI* estimates a degradation level of the composite laminates subjected to repeated impacts, which is proposed as

$$DI = 1-\frac{E^*_{ibs}}{E_{ibs}}. \tag{2}$$

In Eq. (2), E^*_{ibs} and E_{ibs} are the current and initial (for an undamaged specimen) impact bending stiffness. Therefore, *DA* and *DI* are both non-dimensional quantities, with values between 0 (for undamaged material) and 1 (for failed material, at perforation).

The *DA* and *DI* values calculated for four impact energies are presented in Fig. 7. Trends for both *DA* and*DI* prove that the damage accumulation has two different patterns for the mentioned two groups. At impact energies of 2 and 3 J, the damage of tested composite cumulated slowly with an identical pace. For impact energy above 3 J, damage inside the composites increased considerably after each impact. The initiation of fibre failure is reflected in Fig. 7 through an upsurge of both *DA* and *DI* values. A larger impact energy resulted in the higher damage-accumulation rate.

3.2. Damage morphology and delamination under repeated impacts

Together with analysis of mechanical response of the composite to repeated impacts, it is also important to investigate the damage modes and their effects on damage accumulations. Barely visible impact damage (BVID), as a typical damage mode in layered composite materials, can be characterised with Micro-CT scans. Delamination was observed clearly in the cross-section Micro-CT images as a darker zone in Figs. 8–11 (translucency was applied to plies in order to visualize all the damaged interfaces). In addition, surface morphology of tested specimen was also captured and shown in Figs. 8–11 at the same scale as cross-section images. The centre of strike location is positioned at the centre of these figures. The border colour of each image denotes the respective section view of the specimen: green border indicates the plane 1–2; blue – the plane 2–3 and olive - the morphology of the surface 1–2.

Fig. 8(a)–(c) show delamination of the specimen after repeated 2 J impacts. Apparently, no obvious delamination occurred after the first impact; instead, micro-cracks were generated in the matrix-rich zones within interlaced yarns situated around the contact point (Fig. 8(d)). After the second strike, a small range of delamination was captured (Fig. 8(b)). Therefore, the onset of micro-cracks was the first damage mode under repeated impact. Due to a slow damage-accumulation process, the delamination was limited even after 20 impacts. Furthermore, no macroscopic cracks and fibre failure were observed on the surface of the tested specimen (Fig. 8(d)). It indicates that BVID was the main failure mode of the braided composite at impact energy of 2 J.

At impact energy of 3 J, delamination, with a symmetrical dumbbell shape, was observed after the first strike (Fig. 9(a)). Fig. 9(b) and (c) show that this delamination area did not grow too much during the initial four impacts. In contrast to damage caused by 2 J impacts, slight yarn debonding and fibre rupture were observed at the specimen's surface after the 20th impact. Fig. 9(d) illustrates that propagation of delamination led to the growth of inter-yarn cracks. As a consequence, yarn debonding and macroscopic cracks formed on the surface. Although only BVID occurred at such a relative low impact energy, severer damage modes can be generated due to damage accumulation with impacts; the damage modes include plastic deformation, delamination and matrix cracking [17]. Damage within the composites in various modes were regarded as important mechanisms to dissipate energy for braided composites under impact loading. Mouritz et al. [19] inferred that reduction of interfacial shear strength after each impact led to accumulation of matrix cracking, debonding and delamination.

After first four strikes with energy of 4 J, the cracks propagated to the surface of the specimen as a result of delamination and inter-yarn debonding (Fig. 10). The shape of delamination was similar to that of 3 J impacts. On the surface, macro-cracks aligned along the longitudinal yarn direction were also visible, as a result of initial damage induced by bending [20]. It is noticed that fibres in the interlacing yarns broke after 13 impacts, while the delamination and inter-yarn cracks also accumulated. When propagation of cracks is constrained by interlaced yarns, more energy is needed to activate the fibre-failure mode. Hence, the damage-accumulation rate obviously accelerated at

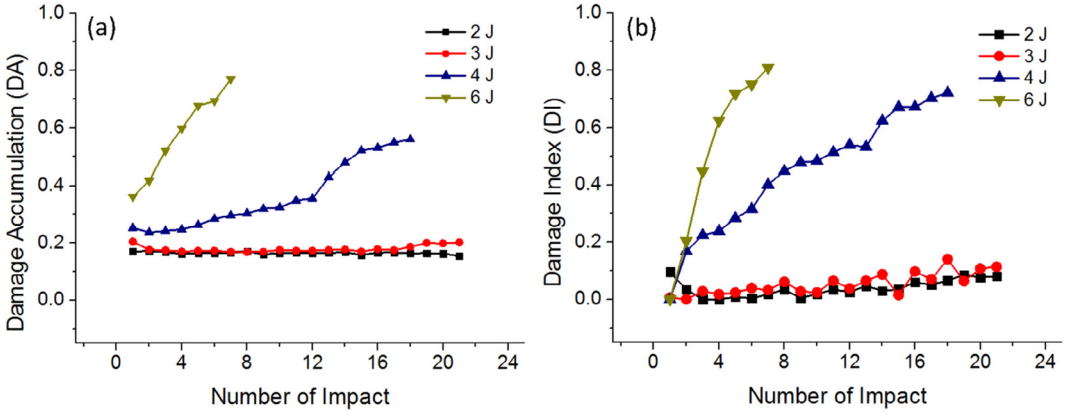

Fig. 7. (a) Damage accumulation (*DA*) parameter and (b) damage index (*DI*) of repeated impacts with different impact energies.

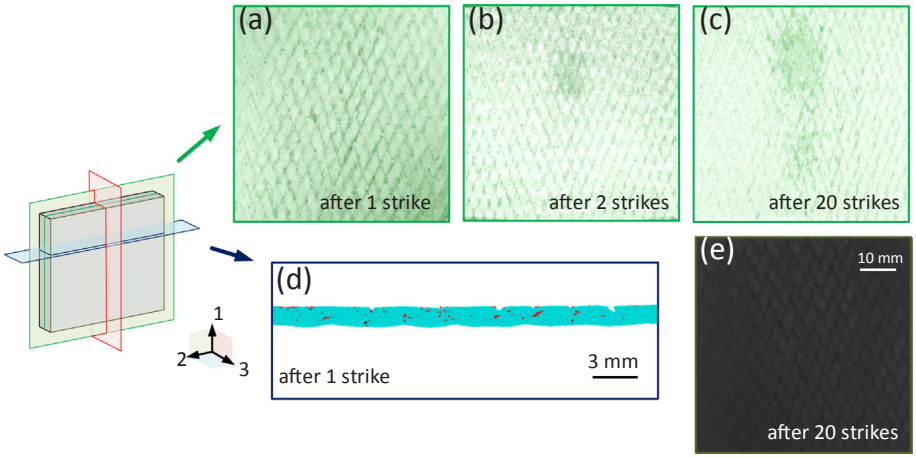

Fig. 8. Micro-CT images of tested braided composite plate under repeated 2 J impacts: (a)–(c) interface delamination; (d) micro-cracks; (e) surface morphology.

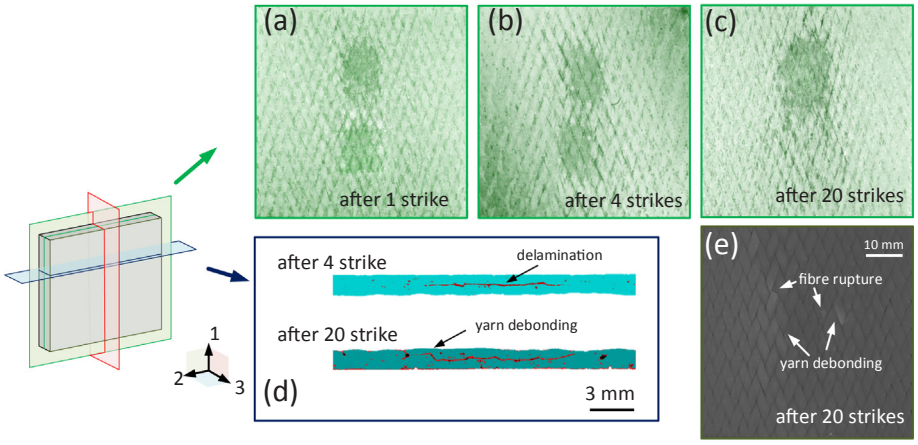

Fig. 9. Micro-CT images of tested braided composite plate under repeated 3 J impacts: (a)–(c) interface delamination, (d) micro-cracks; (e) surface morphology.

this impact-energy level. It is believed that the reduction of bending stiffness is attributed to the extent of impact damage in the specimen, such as delamination and matrix cracking [9]. Above results confirm that the fibre breakages and additional matrix cracks resulted in the sharp reduction in stiffness and contact force, as observed in Figs. 4 and 5(a).

If the impact energy is large enough, multiple impact-damage modes, including matrix cracking, delamination and fibre breakage, occur almost simultaneously after one impact. As shown in Fig. 11(a), the delamination area clearly showed a dumbbell shape after a 6 J impact, propagating along the yarn directions. After a subsequent impact, interfacial cracks start to propagate along the transverse direction with a “W” shape pattern due to hindrance of the interlacing yarns. On the specimen’s surface, longitudinal macroscopic cracks were easily visible after the second impact, while the transverse cracks only occurred on the surface after 6 impacts.

The experimental results revealed that both the impact energy and the number of impacts were the main factors influencing damage accumulation in braided composite exposed to repeated impacts. Depending on the normalised impact energy, material responses to

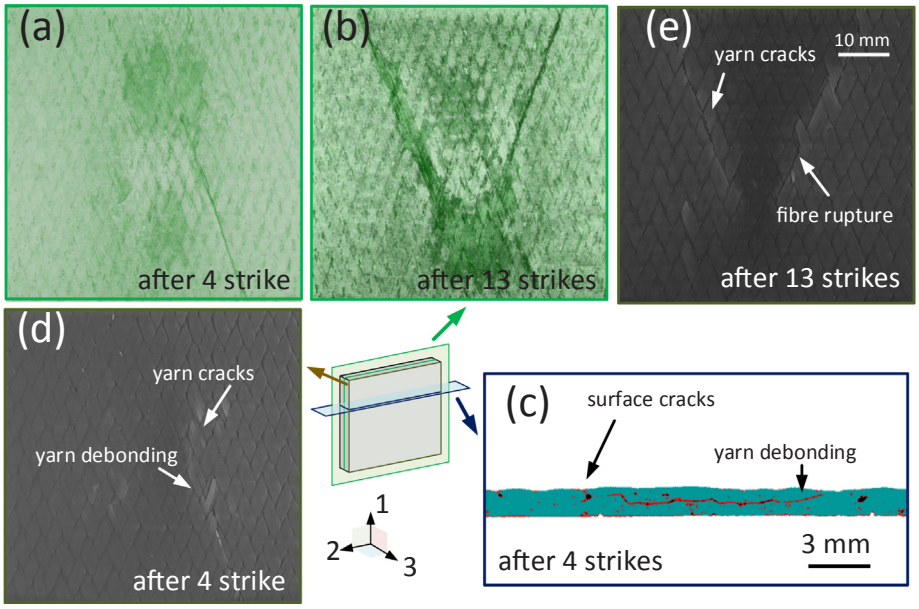

Fig. 10. Micro-CT images of tested braided composite plate under repeated 4 J impacts: (a)–(b) interface delamination, (c) matrix cracking; (d)–(e) surface morphology.

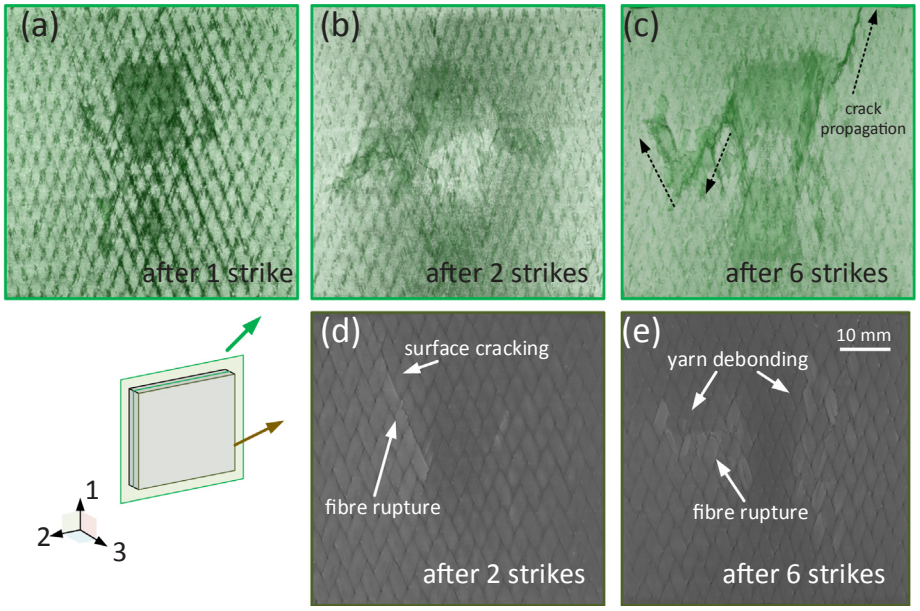

Fig. 11. Micro-CT images of tested braided composite plate under repeated 6 J impacts: (a)–(c) interface delamination; (d)–(e) surface morphology.

repeated impacts had two patterns. The one is a slow damage accumulation corresponding to relatively low normalised impact energies ($E_i/E_p < 0.25$). With an increasing number of impacts, micro-cracks initiated within yarns first, leading to delamination. The damage accumulated so slow that fibre failure mode was only overserved at a small range after quite a few strikes. Hence, bending stiffness decreased at a slow rate, irrespective of impact energy. The initial increment in the peak force is attributed to compaction of a thin and unreinforced matrix layer on the contact surface. Afterwards, the peak load did not change significantly with the number of impacts. On the other hand, repeated impacts with a larger normalised impact energy ($E_i/E_p > 0.3$) can induce severe internal damage [10]. For a rapid damage-accumulation situation, matrix cracking was the first damage mode to occur, immediately followed by fast delamination propagation. The impact bending stiffness and peak load dropped dramatically, since fibre ruptures reduced the stiffness of the composites. After damage accumulation, the macro cracks grew rapidly along the yarn direction and propagated transversely in a “W” pattern with severer fibre rupture.

4. Finite-element modelling of repeated drop-weight impact

The braided composite was modelled employing a multi-scale modelling approach, with information being passed across length-scales [21]. Our previous work [22–25], involving a microscopic model, consisting of hexagonally arranged carbon fibre filaments and polymeric matrix, provided the necessary material constants for the fibre tow. Subsequently, a meso-scale unit cell was used to describe the braided architecture of the fibre bundles and to provide material properties for the macro-scale model. Here, a crucial part of the multi-scale strategy, a physically-based macroscopic model for braided textile-reinforced composites, is presented.

4.1. Progressive damage failure analysis

The Hashin's damage criteria [26,27] are used to model the damage in composites. After damage initiation, the response of the material was computed according to a damage-evolution law based on stress-displacement behaviours of six failure modes. The values of initiation damage criteria $\varnothing_I$ for each type of failure mode I are as follows:

Fibre tensile failure in longitudinal direction $\varnothing_L^t$: ($\sigma_1 \geqslant 0$)

$$\varnothing_L^t = \left(\frac{\sigma_1}{X_T}\right)^2 + \frac{\tau_{12}^2}{(S_{12})^2} + \frac{\tau_{13}^2}{(S_{13})^2} = 1 \tag{3}$$

Fibre compressive failure in longitudinal direction $\varnothing_L^c$: ($\sigma_1 < 0$)

$$\varnothing_L^c = \left(\frac{\sigma_1}{X_C}\right)^2 = 1 \tag{4}$$

Matrix tensile failure in transverse direction $\varnothing_Y^t$: ($\sigma_2 \geqslant 0$)

$$\varnothing_Y^t = \left(\frac{\sigma_2 + \alpha\sigma_3}{Y_T}\right)^2 + \frac{\tau_{23}^2 - \sigma_2\sigma_3}{(S_{23})^2} + \frac{\tau_{12}^2}{(S_{12})^2} + \frac{\tau_{13}^2}{(S_{13})^2} = 1 \tag{5}$$

Matrix compressive failure in transverse direction $\varnothing_Y^c$: ($\sigma_2 < 0$)

$$\varnothing_Y^c = \left[\left(\frac{Y_C}{2S_{23}}\right)^2 - 1\right]\frac{\sigma_2 + \alpha\sigma_3}{Y_C} + \left(\frac{\sigma_2 + \alpha\sigma_3}{2S_{23}}\right)^2 + \frac{\tau_{23}^2 - \sigma_2\sigma_3}{(S_{23})^2} + \frac{\tau_{12}^2}{(S_{12})^2} + \frac{\tau_{13}^2}{(S_{13})^2} = 1 \tag{6}$$

Matrix tensile failure in thickness direction $\varnothing_Z^t$: ($\sigma_3 \geqslant 0$)

$$\varnothing_Z^t = \left(\frac{\sigma_2 + \sigma_3}{Z_T}\right)^2 + \frac{\tau_{23}^2 - \sigma_2\sigma_3}{(S_{23})^2} + \frac{\tau_{12}^2}{(S_{12})^2} + \frac{\tau_{13}^2}{(S_{13})^2} = 1 \tag{7}$$

Matrix compressive failure in thickness direction $\varnothing_Z^c$: ($\sigma_3 < 0$)

$$\varnothing_Z^c = \left[\left(\frac{Z_C}{2S_{23}}\right)^2 - 1\right]\frac{\sigma_2 + \sigma_3}{Z_C} + \left(\frac{\sigma_2 + \sigma_3}{2S_{23}}\right)^2 + \frac{\tau_{23}^2 - \sigma_2\sigma_3}{(S_{23})^2} + \frac{\tau_{12}^2}{(S_{12})^2} + \frac{\tau_{13}^2}{(S_{13})^2} = 1 \tag{8}$$

In Eqs. (3)–(8), X_T, Y_T and Z_T denote tensile strengths in the longitudinal (X), transverse (Y) and through-thickness (Z) directions of the braided composite, respectively. X_C, Y_C and Z_C are compressive strengths in the X, Y and Z directions of the composite, respectively. In indices of stress and strain components, 1, 2 and 3 directions are used to described X, Y and Z, respectively. Hence, S_{12}, S_{13} and S_{23} signify in-plane and two out-of-plane shear strengths, respectively. The effective normal and shear stress components are denoted by σ_i and τ_{ij} ($i, j = 1, 2, 3; i \neq j$), respectively.

For undamaged and elastic orthotropic composite materials, the stress-strain relationship can be written as

$$\begin{Bmatrix}\sigma_{11}\\ \sigma_{22}\\ \sigma_{33}\\ \tau_{12}\\ \tau_{23}\\ \tau_{13}\end{Bmatrix} = \begin{bmatrix} C_{11} & C_{12} & C_{13} & 0 & 0 & 0\\ C_{21} & C_{22} & C_{23} & 0 & 0 & 0\\ C_{31} & C_{32} & C_{33} & 0 & 0 & 0\\ & & & C_{44} & 0 & 0\\ & sym & & & C_{55} & 0\\ & & & & & C_{66}\end{bmatrix}\begin{Bmatrix}\varepsilon_{11}\\ \varepsilon_{22}\\ \varepsilon_{33}\\ \gamma_{12}\\ \gamma_{23}\\ \gamma_{13}\end{Bmatrix}, \tag{9}$$

where σ_{ij} and τ_{ij} are normal and shear stresses, ε_{ij} and γ_{ij} are normal and shear strains, C_{ij} are the stiffness coefficients. According to continuum damage mechanics (CDM), in a finite-element (FE) method, the damage was considered distributed continuously in a finite element, and the ply-damage models assumed that when the values in the initiation damage criteria $\varnothing_I$ were equal to unity, the local stiffness of material C_{ij} degraded. When the constituents of material failed in an element, it dissipated energy equal to its elastic energy. According to Lapczyk and Miami's approach [21,27,28], a characteristic element length was introduced into the expression to solve a mesh-dependence problem. The equivalent displacement at failure point X_{eq}^f was defined as follows:

$$X_{eq}^f = \varepsilon_{If}\, l, \tag{10}$$

where l is the characteristic length of the element and ε_{If} is the equivalent failure strain of failure mode I. Thus, degradation of stiffness tensors was characterized by a damage matrix, $\boldsymbol{C}(\boldsymbol{D})$, defined by internal damage variables d_I associated to different failure modes I [29]. The damage variable of each failure mode is expressed by the following equivalent displacement:

$$d_I = \frac{X_{eq}^{If}(X_{eq}^I - X_{eq}^{Ii})}{X_{eq}^I(X_{eq}^{If} - X_{eq}^{Ii})} (I = Lt, Lc, Yt, Yc, Zt, Zc). \tag{11}$$

In Eq. (11), X_{eq}^{Ii} and X_{eq}^{If} are the initiation and full-damage equivalent displacements of failure mode I, respectively. X_{eq}^{Ii} and X_{eq}^{If} can be calculated with the following equations [30]:

$$X_{eq}^{Ii} = \frac{X_{eq}^I}{\sqrt{\varnothing_I}}, \tag{12}$$

$$X_{eq}^{If} = \frac{2G_I}{\sigma_{eq}^{Ii}}. \tag{13}$$

Here, $\varnothing_I$ is the value of the initiation damage criteria. G_I and σ_{eq}^{Ii} denote the fracture energy density and the initiation damage equivalent stress of failure mode I, respectively. The initiation equivalent stress σ_{eq}^{Ii} can be calculated from the following equation:

$$\sigma_{eq}^{Ii} = \frac{\sigma_{eq}^I}{\sqrt{\varnothing_I}}. \tag{14}$$

In Eqs. (11)–(14), the equivalent stress σ_{eq}^I and the equivalent displacement X_{eq}^I associated to the different failure modes are expressed in Table 1. The equivalent displacements of initiation damage listed in Table 1 have the similar forms with Eq. (10).

Therefore, the damage evolution equation is associated with the characteristic element length, local strain and fracture energy of the

Table 1
Equivalent displacements and stresses corresponding to different failure modes.

Failure mode I	Equivalent displacement	Equivalent stress
L_t, $\sigma_1 \geq 0$	$X_{eq}^{Lt} = l\sqrt{<\varepsilon_{11}>^2 + \varepsilon_{12}^2 + \alpha\varepsilon_{31}^2}$	$l(<\sigma_{11}><\varepsilon_{11}> + \sigma_{12}\varepsilon_{12} + \alpha\sigma_{13}\varepsilon_{13})/X_{eq}^{Lt}$
L_c, $\sigma_1 < 0$	$X_{eq}^{Lc} = l<-\varepsilon_{11}>$	$l(<-\sigma_{11}><-\varepsilon_{11}>)/X_{eq}^{Lc}$
Y_t, $\sigma_2 \geq 0$	$X_{eq}^{Yt} = l\sqrt{<\varepsilon_{22}>^2 + \varepsilon_{12}^2 + \alpha\varepsilon_{23}^2}$	$l(<\sigma_{22}><\varepsilon_{22}> + \sigma_{12}\varepsilon_{12} + \alpha\sigma_{23}\varepsilon_{23})/X_{eq}^{Yt}$
Y_c, $\sigma_2 < 0$	$X_{eq}^{Yc} = l<-\varepsilon_{22}>$	$l(<-\sigma_{22}><-\varepsilon_{22}>)/X_{eq}^{Yc}$
Z_t, $\sigma_3 \geq 0$	$X_{eq}^{Zt} = l\sqrt{<\varepsilon_{33}>^2 + \varepsilon_{23}^2 + \varepsilon_{31}^2}$	$l(<\sigma_{33}><\varepsilon_{33}> + \sigma_{23}\varepsilon_{23} + \sigma_{13}\varepsilon_{13})/X_{eq}^{Zt}$
Z_c, $\sigma_3 < 0$	$X_{eq}^{Zc} = l<-\varepsilon_{33}>$	$l(\nu_{23}(<-\sigma_{33}><-\varepsilon_{33}>)/X_{eq}^{Zc}$
$<x> = (x + \lvert x\rvert)/2$		

braided-composite constituents. The damaged stiffness matrix $\boldsymbol{C}(\boldsymbol{D})$ can be expressed in a matrix form by using the components of undamaged stiffness matrix and the principal values of the damage tensor D_I according to the Murakami-Ohno damage model [31]. It can be presented more explicitly as follows:

$$C(D) = \begin{bmatrix} b_L^2 C_{11} & & b_L b_T C_{12} & b_L b_Z C_{13} & 0 & 0 & 0 \\ & & b_T^2 C_{22} & b_T b_Z C_{23} & 0 & 0 & 0 \\ & & & b_Z^2 C_{33} & 0 & 0 & 0 \\ & sym & & & b_{LT} C_{44} & 0 & 0 \\ & & & & & b_{TZ} C_{55} & 0 \\ & & & & & & b_{ZL} C_{66} \end{bmatrix}, \tag{15}$$

where $b_L = 1-D_L$, $b_T = 1-D_T$, $b_Z = 1-D_Z$,

$$b_{LT} = \left(\frac{2(1-D_L)(1-D_T)}{2-D_L-D_T}\right)^2, \; b_{TZ} = \left(\frac{2(1-D_T)(1-D_Z)}{2-D_T-D_Z}\right)^2, \; b_{ZL} = \left(\frac{2(1-D_Z)(1-D_L)}{2-D_Z-D_L}\right)^2$$

,

C_{ij} $(i, j = 1, 2, 3)$ is the component of the undamaged stiffness matrix, $D_L = \max(d_{Lt}, d_{Lc})$, $D_T = \max(d_{Tt}, d_{Tc})$, $D_Z = \max(d_{Zt}, d_{Zc})$.

4.2. Cohesive-zone model

Delamination between layers in the composite was simulated with the interface cohesive-zone model, defined by a traction-separation constitutive law. This law describes an initial linear-elastic stage until a damage-initiation condition is satisfied, followed by a linear softening phase simulating progressive de-cohesion of the interface with increasing damage. According to the law, the area under the traction-displacement curve represents fracture toughness (the critical energy release rate) for a specific fracture mode [32]. Complete fracture of the interface is assumed to occur when the cohesive traction vanishes at the end of the degradation phase. The evolution of damage in simulations was monitored by a damage indicator, ranging from 0 for the undamaged interface to the value of 1 implying complete de-cohesion of the interface. The crack was initiated when a stress-based quadratic interaction criterion was satisfied:

$$\left(\frac{t_n}{N}\right)^2 + \left(\frac{t_s}{S}\right)^2 + \left(\frac{t_t}{S}\right)^2 = 1, \tag{16}$$

where t_n, t_s, t_t represent the interface stresses and N, S, T are the interface strengths under mode I (opening), mode II (shear) and mode III (tearing), respectively. The values of N and S were selected in a preliminary calibration phase based on comparison of experimental data and results of simulations of the interfacial study [33].

Damage evolution was defined based on fracture energy, and a linear softening behaviour was utilised. The dependency of fracture energy on mixed fracture modes was expressed by the widely used Benzeggagh-Kenane formulation [34]:

$$G^C = G_n^C + (G_s^C - G_n^C)\left\{\frac{G_s^C + G_t^C}{G_n^C + G_s^C + G_t^C}\right\}^\eta, \tag{17}$$

where G_n, G_s and G_t are the work done by tractions and their conjugate relative displacements corresponding to modes I, II and III, respectively. The power, η, is a material parameter, selected as 1.45 for a carbon-fibre composite [35].

4.3. Drop-weight test model

The braided composite plate was modelled as a homogeneous material in a macroscopic formulation, as shown in Fig. 12. The circular pneumatic clamps used in the testing machine were simulated as rigid bodies (R3D4) with their original geometry. The nodes at the model's periphery were fixed in all directions to mimic the experimental process, where the composite plate was pneumatically clamped, as marked in Fig. 12. The dimensions of the model were the same as of the employed experimental setup. The spike-shaped impactor was modelled as a rigid body with a lumped mass equal to the mass used in the experimental programme. A general contact algorithm was defined with appropriate contact-pair properties to represent the contact between the impactor and the composite-plate surface. Levels of initial velocity in the vertical direction are prescribed for the impactor, resulting in the corresponding impact energy of 2, 3, 4 and 6 J. the impactors impacted and rebounded successively, with the same initial velocity. For each impact energy level, the drop-weight impact was repeated for six times. The material properties used in this study are listed in Table 2.

In this study, an element-based cohesive zone (ECZ) modelling technique was adopted. In the ECZ model, cohesive elements (COH3D8) with thickness of 0.01 mm were inserted between two plies of the composite. These cohesive-zone elements shared the nodes of the adjacent composite layers. To consider out-of-plane stress components, 3D stress elements (C3D8R) were incorporated in the composite layers instead of shell elements in the ECZ model. Here, the impact-induced damage was modelled by implementing a user-defined 3D damage model (Eqs. (1)–(10)) in a VUMAT subroutine of ABAQUS/Explicit.

4.4. Simulation results and discussion

FE predictions and experimental results were compared in terms of the global response and delamination damage for four impact energy levels. The global responses of the composite were mainly characterised with regard to the peak impact force, absorbed energy and damage accumulation. Fig. 13 gives examples of the representative load- and energy-time curves obtained by both experimental and numerical methods when the impact energy keeps 3 J. In fact, for all the impact energy levels studied herein, the predicted levels of peak forces and absorbed energy were found to agree well with the experimental data, not only for the initial impact, but also after 6 times of impacts.

Computational results for six times impacts at impact energy of 2 J are presented in Fig. 14. The trends of global responses are well captured reasonably by the simulations. The peak load and absorbed energy keep their stable levels after repeated impacts. The predicted absorbed energy is slightly lower than that from experimental observations, indicating that the internal damage of the composites (*i.e.* matrix cracking failure) was underestimated at impact energy of 2 J. At this impact energy level, nearly constant damage-accumulation parameters were obtained both experimentally and numerically, which is consistent with the fact that no significant accumulation of damage occurred except for initial specimen indentation. Meanwhile, a symmetrical dumbbell-shape delamination area was captured with the developed FE method. It is obvious that the damage contours are mainly along the longitudinal direction. This also agreed well with the experiments where matrix cracks initiated around the impact area and propagated along the yarns direction. According to Fig. 14(d), the delamination area increased slightly after repeated impact with stable shapes.

The results predicted for impact energy of 3 J are shown in Fig. 15. Overall, the trends of FE results are reasonable, compared with the experimentally obtained peak loads and absorbed energy. Damage accumulation from the FE simulation was higher because, in the repeated impacts, failure elements have lower stiffness to bear impact loading. Since the impactor was in contact with the relatively soft material, the extent of deformation was more obvious in simulations. The delamination area increased significantly after two strikes, and then grew slightly for the subsequent impacts. This phenomenon was confirmed by micro-CT scans as well. Wyrick et al. [37] also reported that the main damage in carbon/epoxy composites occurred during the few initial impacts, and subsequent impacts led to smaller damage

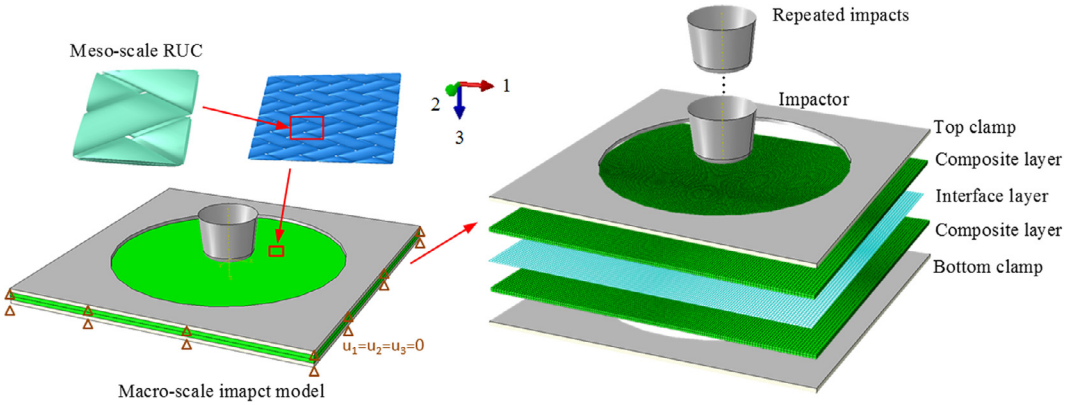

Fig. 12. FE drop-weight impact model with spike-shape impactor: from meso-scale to macro-scale model.

Table 2
Material properties used in FE model.

Layer properties [22–25] (A-42/L20)	E_{11} = 36.37 GPa; E_{22} = 7.4 GPa, E_{33} = 7.07 GPa; ν_{12} = 1.19; ν_{13} = 0.026; ν_{23} = 0.29; G_{12} = 16.31 GPa; G_{13} = 2.72 GPa; G_{23} = 2.31 GPa; X_t = 591.57 MPa; X_c = 400 MPa; Y_t = 200 MPa; Y_c = 275 MPa; Z_t = 190 MPa, Z_c = 270 MPa; G_{ft} = 81.5 kJ/m^2; G_{fc} = 100 kJ/m^2; G_{mt} = 33 kJ/m^2; G_{mc} = 33 kJ/m^2;
Layer interface properties [24,35,36]	k_N = 289 GPa/mm; k_S = k_T = 200 GPa/mm N = 58.3 MPa; S = T = 62.3 MPa; G_{Ic} = 350 J/m^2; G_{IIc} = G_{IIIc} = 1000 J/m^2

increments. Both compression closure and highly localized damage resulted in a saturation of delamination area. In addition, this indicates that the energy absorbed in delamination was less significant after a certain number of strikes. Instead, other types of damage, including matrix cracking, fibre fracture and even perforation, were generated [38]. Specifically for textile composites, the growth of delamination area was also restricted by their high structural integrity [6,30].

For the impact energy of 4 J, the FE model demonstrated its capability to capture a response of the braided composite to repeated impacts, with a good correlation with the experimental observations. In Fig. 16, both increasing trends for the peak force and damage accumulation are captured by the developed numerical method. For six impacts, the absorbed energies still keep its flat trend, indicating that there is no fibre failure mode induced in the composite, and damage accumulation is slow. Delamination is still the most important damage mode in the composite material to dissipate energy at this impact-

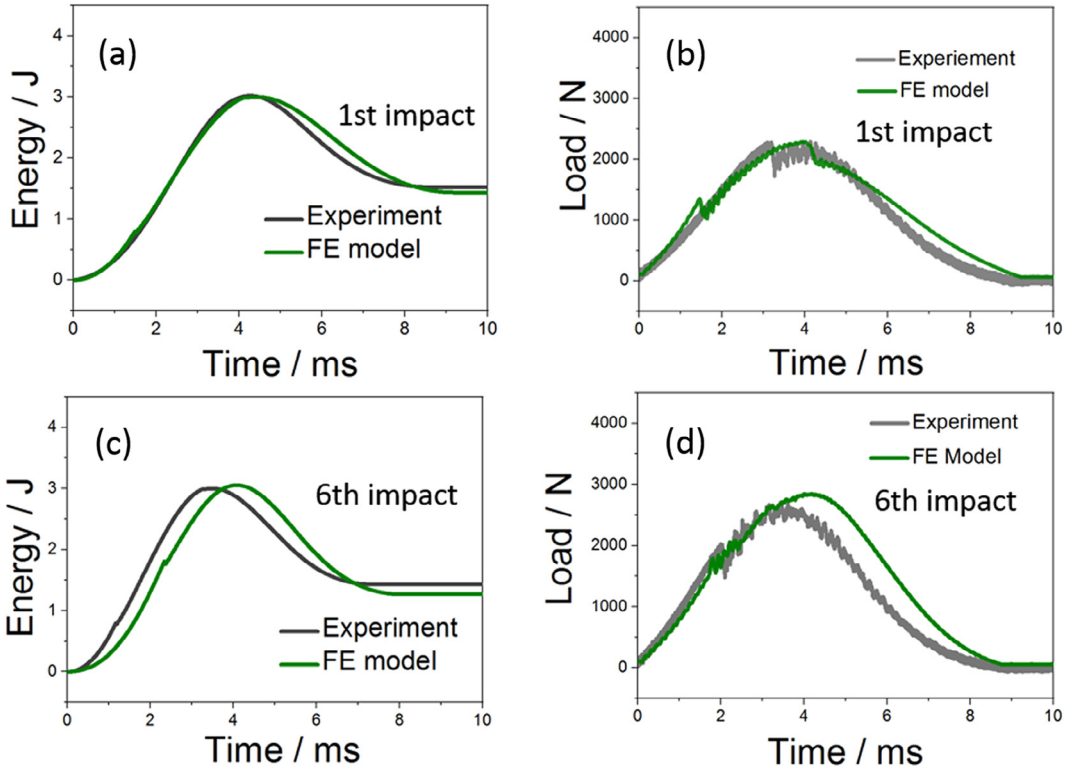

Fig. 13. Representative energy-time and load-time responses of braided composite plate under 3 J repeated impact: (a) and (b) the 1st impact; (c) and (d) the 6th impact.

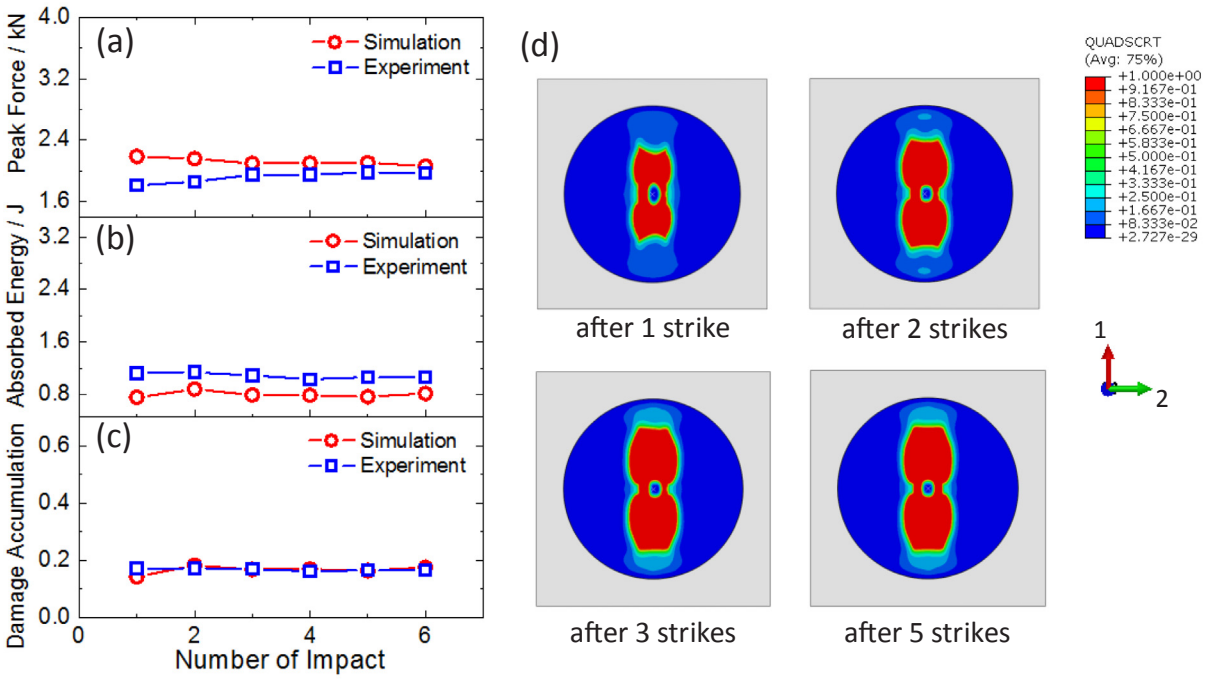

Fig. 14. Simulation results corresponding to repeated impacts at impact energy of 2 J: (a) peak force; (b) absorbed energy; (c) damage accumulation; (d) evolution of delamination in braided composite plate.

energy level. The predicted delamination shape agreed well with the images acquired with CT-scans, as shown in Fig. 16(d). The area of delamination increased with the impact energy, and was close to a saturation value after three strikes. Azouaoui et al. [38] suggested that delamination saturation appeared when there was no new damage developed so that the propagation of delamination stopped after a certain number of impacts.

The predicted areas of delamination were quantified and plotted as a function of impact energy (Fig. 17); apparently, higher impact energy leads to a larger delamination area. Generally, the interface damage propagated rapidly in the second impact, and continued to increase in smaller increments under subsequent impacts. Therefore, the trend for the delamination area can be fitted as an exponential curve, as presented in Fig. 17. This trend agreed well with other experimental works [6,30,39,40], stating that after a certain number of impacts delamination area does not increase significantly. It is also noted in our previous

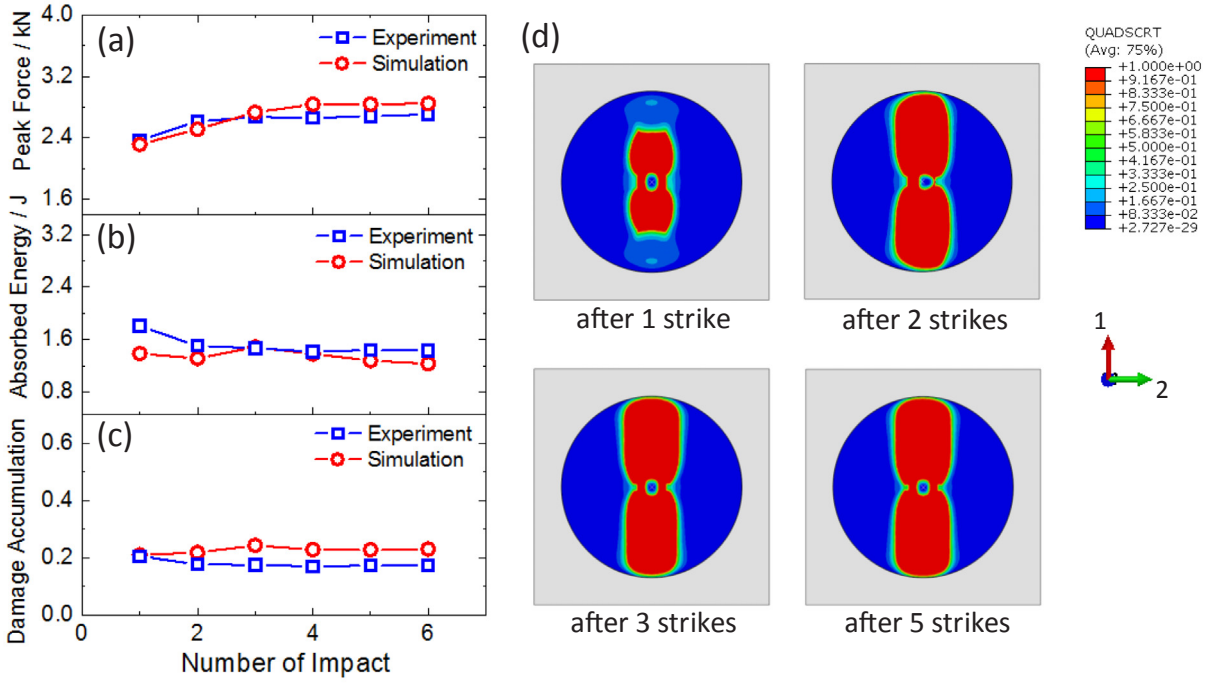

Fig. 15. Simulation results corresponding to repeated impacts at impact energy of 3 J: (a) peak force; (b) absorbed energy; (c) damage accumulation; (d) evolution of delamination in braided composite plate.

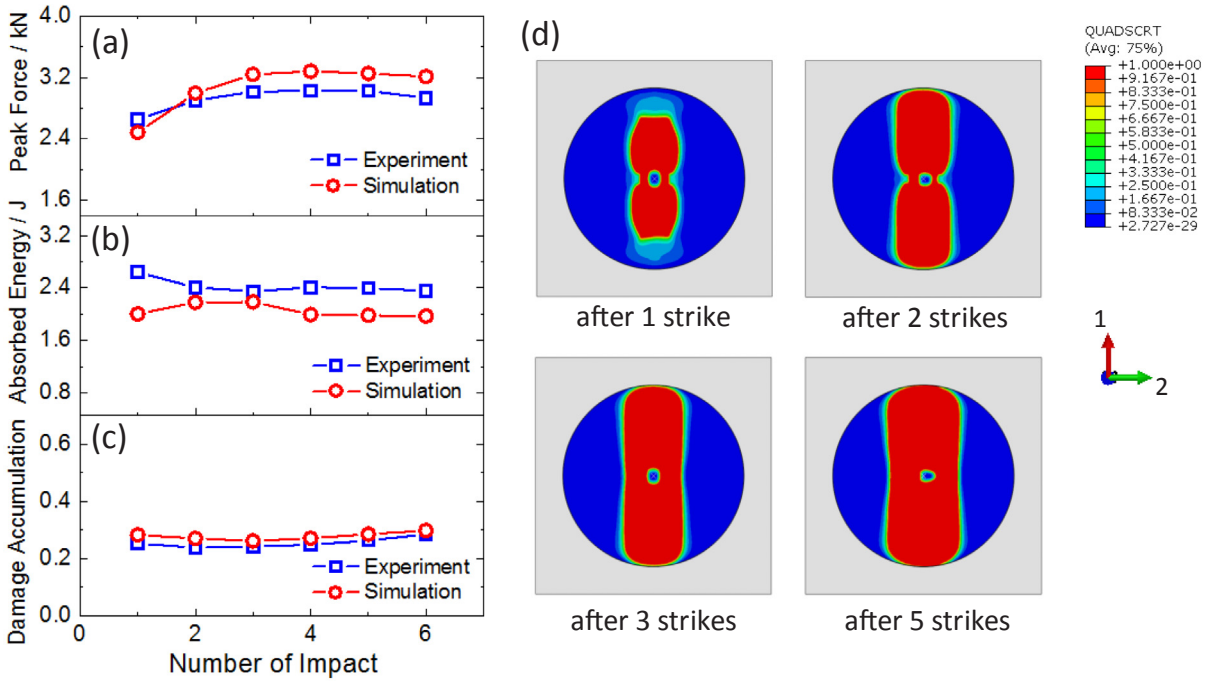

Fig. 16. Simulation results corresponding to repeated impacts at impact energy of 4 J: (a) peak force; (b) absorbed energy; (c) damage accumulation; (d) evolution of delamination in braided composite plate.

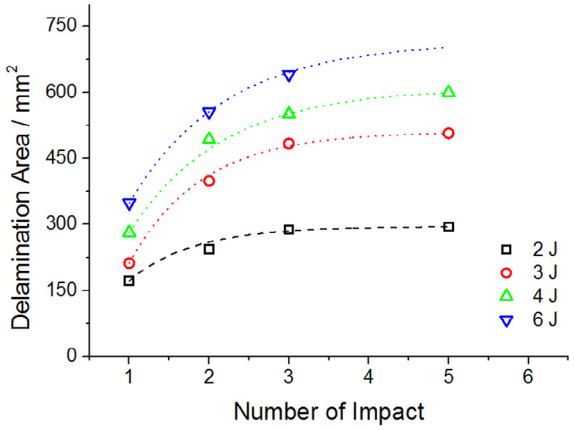

Fig. 17. Predicted delamination area as function of impact number.

studies [23,25] that the performance of braided composites strongly depends on interface properties. For protective applications, interfacial shear strength and fracture toughness of fibre/matrix interface are key to optimize energy absorption performance, as well as structural integrity, of braided composites. With a successfully developed multi-scale modelling capability, it is possible to link individual component with performance of final composite products, which enhanced design of such composite materials.

5. Conclusions

The responses of the braided composite to repeated low-velocity impacts were investigated both experimentally and with FE simulations; the impact-energy level ranged from 2 J to 6 J. The experimental results show that material responses to repeated impacts have two types depending on the normalised impact energy. Referring to relatively low normalised impact energies ($E_i/E_p < 0.25$), bending stiffness decreased with a slow rate with subsequent impacts. The peak load did not change significantly after a slight increment at the initial few impacts, which was the result of the compaction of the unreinforced matrix layer. Almost the same amount of energy was dissipated for each impact. On the other hand, a larger normalised impact energy ($E_i/E_p > 0.3$) can induce server internal damage, with more energy absorbed. The impact bending stiffness and the peak load diminished dramatically in this case, since the fibre breakage decreased the local rigidity at the impact point.

In addition, damage accumulation of braided composites associated with different failure modes was also evaluated. These mechanisms are micro-cracks, delamination, matrix failure, fibre breakage and, uniquely for the braided composite, inter-yarn debonding. When impact energy was low, micro-cracks were initiated within yarns first, leading to the dominant failure mode of delamination. The damage accumulated so slow that the fibre-failure mode could be only observed at a small range after quite a few strikes. In contrast, under impacts with a higher energy, matrix cracking was the first damage mode, immediately followed by fast delamination propagation. After swift damage accumulation, the macro cracks grew rapidly along the yarn direction and propagated transversely in a "W" pattern with severer fibre ruptures.

Furthermore, finite-element modelling capability for analysis of repeated impacts was presented. The computed results show reasonable agreements with the original experimental data in terms of peak load, absorbed energy and maximum deflection of each impact. The damage-accumulation factors with increasing trends were also predicted by the FE method. Applying element-based cohesive-zone models, delamination areas can be predicted; the numerical results showed that delamination propagated rapidly after the first impact. In successive impacts, the delamination area increased at a lower rate, finally moving to a saturate value.

Acknowledgment

The work was supported by the Institute for Sports Research (ISR) at Nangyang Technological University (NTU) through a research scholarship. CW is also grateful for the collaboration with the Mechanics of Advanced Materials (MoAM) Research Group and Sports Technology Institute (STI) at Loughborough University, UK.

References

[1] Lopes CS, Camanho PP, Gürdal Z, Maimí P, González EV. Low-velocity impact damage on dispersed stacking sequence laminates. Part II: Numerical simulations. Compos Sci Technol 2009;69(7–8):937–47.

[2] Schwab M, Todt M, Wolfahrt M, Pettermann HE. Failure mechanism based modelling of impact on fabric reinforced composite laminates based on shell elements. Compos Sci Technol 2016;128:131–7.

[3] Hou JP, Petrinic N, Ruiz C, Hallett SR. Prediction of impact damage in composite plates. Compos Sci Technol 2000;60(2):273–81.

[4] Alemi-Ardakani M, Milani AS, Yannacopoulos S, Borazghi H. A rapid approach for predication and discrete lay-up optimization of glass fiber/polypropylene composite laminates under impact. Int J Impact Eng 2015;84:134–44.

[5] Icten BM. Repeated impact behavior of glass/epoxy laminates. Polym Compos 2009;30(11):1562–9.

[6] Hosur MV, Karim MR, Jeelani S. Experimental investigations on the response of stitched/unstitched woven S2-glass/SC15 epoxy composites under single and repeated low velocity impact loading. Compos Struct 2003;61(1–2):89–102.

[7] Aurrekoetxea J, Sarrionandia M, Mateos M, Aretxabaleta L. Repeated low energy impact behaviour of self-reinforced polypropylene composites. Polym Test 2011;30(2):216–21.

[8] David-West OS, Nash DH, Banks WM. An experimental study of damage accumulation in balanced CFRP laminates due to repeated impact. Compos Struct 2008;83(3):247–58.

[9] Atas C, Icten BM, Küçük M. Thickness effect on repeated impact response of woven fabric composite plates. Compos B Eng 2013;49:80–5.

[10] Tian S, Zhou Z. New criteria for simulating failure under multiple impacts of the same total energy on glass fiber reinforced aluminum alloy laminates. Mater Des 2016;102:142–50.

[11] Bora MÖ, Çoban O, Sinmazçelik T, Cürgül İ, Günay V. On the life time prediction of repeatedly impacted thermoplastic matrix composites. Mater Des 2009;30(1):145–53.

[12] Belingardi G, Cavatorta MP, Paolino DS. On the rate of growth and extent of the steady damage accumulation phase in repeated impact tests. Compos Sci Technol 2009;69(11–12):1693–8.

[13] Amaro AM, Reis PN, De Moura MF, Neto MA. Influence of multi-impacts on GFRP composites laminates. Compos B Eng 2013;52:93–9.

[14] Wang C, Roy A, Silberschmidt VV, Chen Z. Modelling of damage evolution in braided composites: recent developments. Mech Adv Mater Modern Process 2017;3(1):15.

[15] Icten BM. Low temperature effect on single and repeated impact behavior of woven glass-epoxy composite plates. J Compos Mater 2015;49(10):1171–8.

[16] Sevkat E, Liaw B, Delale F, Raju BB. Effect of repeated impacts on the response of plain-woven hybrid composites. Compos B Eng 2010;41(5):403–13.

[17] Belingardi G, Cavatorta MP, Paolino DS. Repeated impact response of hand lay-up and vacuum infusion thick glass reinforced laminates. Int J Impact Eng 2008;35(7):609–19.

[18] Amaro AM, Reis PN, Neto MA. Experimental study of temperature effects on composite laminates subjected to multi-impacts. Compos B Eng 2016;98:23–9.

[19] Mouritz AP, Gallagher J, Goodwin AA. Flexural strength and interlaminar shear strength of stitched GRP laminates following repeated impacts. Compos Sci Technol 1997;57(5):509–22.

[20] De Moura MF, Gonçalves JP. Modelling the interaction between matrix cracking and delamination in carbon–epoxy laminates under low velocity impact. Compos Sci Technol 2004;64(7–8):1021–7.

[21] Lorca J, González C, Molina-Aldareguía JM, Segurado J, Seltzer R, Sket F, et al. Multiscale modeling of composite materials: a roadmap towards virtual testing. Adv Mater 2011;23(44):5130–47.

[22] Ji X, Wang C, Francis BA, Chia ES, Zheng L, Yang J, et al. Mechanical and interfacial properties characterisation of single carbon fibres for composite applications. Exp Mech 2015;55(6):1057–65.

[23] Wang C, Zhong YC, Adaikalaraj PFB, Ji XB, Roy A, Silberschmidt VV, Chen Z. Strength prediction for bi-axial braided composites by a multi-scale modelling approach. J Mater Sci 2016;51:6002–18.

[24] Wang C, Ji X, Roy A, Silberschmidt VV, Chen Z. Shear strength and fracture toughness of carbon fibre/epoxy interface: effect of surface treatment. Mater Des 2015;85:800–7.

[25] Wang C, Roy A, Chen Z, Silberschmidt VV. Braided textile composites for sports protection: energy absorption and delamination in impact modelling. Mater Des 2017;136:258–69.

[26] Hashin Z. Fatigue failure criteria for unidirectional fiber composites. J Appl Mech 1981;48(4):846–52.

[27] Lapczyk I, Hurtado JA. Progressive damage modeling in fiber-reinforced materials. Compos A Appl Sci Manuf 2007;38(11):2333–41.

[28] Maimı P, Camanho PP, Mayugo JA, Dávila CG. A continuum damage model for composite laminates: part II–computational implementation and validation. Mech Mater 2007;39(10):909–19.

[29] Guo-dong F, Jun L, Bao-lai W. Progressive damage and nonlinear analysis of 3D four-directional braided composites under unidirectional tension. Compos Struct 2009;89(1):126–33.

[30] Kang H, Shan Z, Zang Y, Liu F. Progressive damage analysis and strength properties of fiber-bar composites reinforced by three-dimensional weaving under uniaxial tension. Compos Struct 2016;141:264–81.

[31] Murakami S. Mechanical modeling of material damage. J Appl Mech 1988;55(2):280–6.

[32] Singh H, Mahajan P. Modeling damage induced plasticity for low velocity impact simulation of three dimensional fiber reinforced composite. Compos Struct 2015;131:290–303.

[33] Camanho PP, Davila CG, De Moura MF. Numerical simulation of mixed-mode progressive delamination in composite materials. J Compos Mater 2003;37(16):1415–38.

[34] Benzeggagh ML, Kenane M. Measurement of mixed-mode delamination fracture toughness of unidirectional glass/epoxy composites with mixed-mode bending apparatus. Compos Sci Technol 1996;56(4):439–49.

[35] González EV, Maimí P, Camanho PP, Turon A, Mayugo JA. Simulation of drop-weight impact and compression after impact tests on composite laminates. Compos Struct 2012;94(11):3364–78.

[36] Shi Y, Pinna C, Soutis C. Modelling impact damage in composite laminates: a simulation of intra-and inter-laminar cracking. Compos Struct 2014;114:10–9.

[37] Wyrick DA, Adams DF. Damage sustained by a carbon/epoxy composite material subjected to repeated impact. Composites 1988;19(1):19–27.

[38] Azouaoui K, Rechak S, Azari Z, Benmedakhene S, Laksimi A, Pluvinage G. Modelling of damage and failure of glass/epoxy composite plates subject to impact fatigue. Int J Fatigue 2001;23(10):877–85.

[39] Baucom JA, Zikry MA. Low-velocity impact damage progression in woven E-glass composite systems. Compos A Appl Sci Manuf 2005;36(5):658–64.

[40] Tooski MY, Alderliesten RC, Ghajar R, Khalili SM. Experimental investigation on distance effects in repeated low velocity impact on fiber–metal laminates. Compos Struct 2013;99:31–40.